

Synthesis and characterization of new ruthenium complexes with active ligands against Chagas' disease

Lucía Otero^{a,*}, Pabla Noblia^a, Dinorah Gambino^{a,*}, Hugo Cerecetto^b, Mercedes González^b, Javier A. Ellena^c, Oscar E. Piro^d

^a Cátedra de Química Inorgánica, Facultad de Química, Universidad de la República, Gral Flores 2124, C.C. 1157, 11800 Montevideo, Uruguay

^b Departamento de Química Orgánica, Facultad de Química-Facultad de Ciencias, Universidad de la República, Gral Flores 2124, C.C. 1157, 11800 Montevideo, Uruguay

^c Instituto de Física de São Carlos, Universidade de São Paulo, C.P. 369, 13560 São Carlos (SP), Brazil

^d Departamento de Física, Facultad de Ciencias Exactas, Universidad Nacional de La Plata and Instituto IFLP (CONICET), C.C. 67, 1900 La Plata, Argentina

Received 13 May 2002; accepted 4 September 2002

Abstract

Chagas' disease, considered incurable, is a major third world parasitosis that affects millions of people in Latin America. Previous work has shown that ruthenium clotrimazole complexes are more active against *Trypanosoma cruzi*, causative agent of Chagas' disease, than the corresponding free ligand. In this work, the synthesis and characterization of a series of new Ru(II) complexes with different antitrypanosomal active compounds is presented. Complexes of general formulae $[\text{Ru}^{\text{II}}\text{Cl}_2(\text{dmsO})_2\text{L}]$, where dmsO = dimethylsulfoxide and L = 5-nitro-2-furaldehyde semicarbazone (**L1**), *N*⁴-*n*-butyl-5-nitro-2-furaldehyde semicarbazone (**L2**) or 3-(5-nitrofuryl)acroleine semicarbazone (**L3**), were prepared in good yields by reaction of $[\text{Ru}^{\text{II}}\text{Cl}_2(\text{dmsO})_4]$ with L in ethanol or toluene solutions. Complexes were characterized by elemental analyses and electronic, FTIR, ¹H and ¹³C NMR spectroscopies. Crystal and molecular structures of $[\text{RuCl}_2(\text{dmsO})_2\text{L1}]$ and $[\text{RuCl}_2(\text{dmsO})_2\text{L2}]$ were determined by X-ray diffraction methods. In both crystals the ruthenium metal atom is in a quite similar elongated octahedral environment, equatorially coordinated to the semicarbazone molecule, acting as a bidentate ligand through its azomethinic nitrogen and carbonylic oxygen atoms. The sixfold coordination is completed with the sulfur atoms of two dimethylsulfoxide ligands at *cis* positions and two chlorine ions at the axial positions. The proposed formula for **L3** complex was supported by FTIR, NMR and theoretical studies. NOE–NMR experiments allowed to assign **L3** spatial distribution in the complex.

© 2002 Elsevier Science B.V. All rights reserved.

Keywords: Ruthenium complexes; Semicarbazone complexes; Chagas' disease chemotherapy

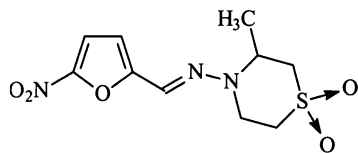
1. Introduction

Chagas' disease is a major third world parasitic disease that affects millions of people in Latin America. It represents a serious problem for public health as there are currently no satisfactory methods of immunoprophylaxis or chemotherapy. The main drug in use is NifurtimoxTM (Fig. 1) but it has undesirable side effects and it is yet inefficient in treating the chronic state of the

disease [1,2]. In this context, some semicarbazones derived from 5-nitrofurfural have been synthesized and they have shown activity against *Trypanosoma cruzi*, causative agent of Chagas' disease. On one hand, and as it is suggested for NifurtimoxTM, these compounds have proved to generate nitro anion radicals that may be responsible of their action against *T. cruzi* [3,4]. On the other hand, there exists a remarkable coincidence between metal drugs which are active trypanocides and active antitumor agents. This is probably attributable to a similarity between the metabolism of tumor cells and pathogenic trypanosomes [5]. In particular, the use of ruthenium complexes as chemo-therapeutic agents is

* Corresponding authors.

E-mail address: dgambino@fq.edu.uy (D. Gambino).

Fig. 1. Formula of NifurtimoxTM.

also well-established in the treatment of cancer [6]. Moreover, previous work has shown that some metal complexes of certain anti-trypanosomal drugs (imidazole and thiazole derivatives) resulted to be more active than the corresponding free ligands [7–11]. Consequently, a successful approach towards the development of new agents against Chagas' disease has been the synthesis of ruthenium complexes with ligands bearing anti-trypanosomal activity [7,9].

In this work, we have developed new Ru(II) complexes with Nitrofurazone (**RuL1**) and its derivatives *N*⁴-*n*-butyl-5-nitro-2-furaldehyde semicarbazone (**RuL2**) and 3-(5-nitrofuryl)acroleine semicarbazone (**RuL3**) as ligands, in an effort to combine free ligand and metal potential antitrypanosomal activities [7,9,12,13]. Ligand formula are depicted in Fig. 2.

From the chemical point of view, it is interesting to note that although metal complexes of semicarbazones have received some attention, ruthenium complexes of such ligands still remain scarcely studied [14].

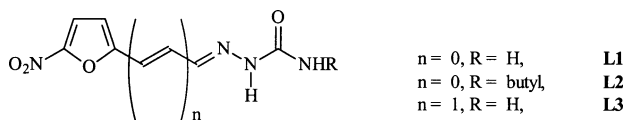


Fig. 2. Formula of the semicarbazone derivatives used as ligands.

2. Experimental

All common laboratory chemicals were purchased from commercial sources and used without further purification. 5-Nitro-2-furaldehyde semicarbazone (Nitrofurazone) was commercially available. *N*⁴-*n*-Butyl-5-nitro-2-furaldehyde semicarbazone and [Ru^{II}Cl₂(dmsO)₄] were prepared according to literature procedures [4,15].

2.1. Synthesis of 3-(5-nitrofuryl)acroleine semicarbazone

A mixture of 3-(5-nitro-2-furyl)acroleine (1.00 g, 5.99 mmol), semicarbazide hydrochloride (0.66 g, 5.99 mmol) and *p*-TsOH (catalytic amounts) in anhydrous toluene (5.0 ml) was stirred at room temperature (r.t.) until no aldehyde was present (checked by TLC on SiO₂, petroleum ether:EtOAc (1:1)). The solid precipitated was filtered off and purified by chromatography (SiO₂, CH₂Cl₂:MeOH (95:5)). The fraction corresponding to

the product was crystallized from EtOH, yielding yellow–orange needles (0.74 g, 55%). ¹H-NMR (dmsO-d₆, 400 MHz): δ 6.40 (bs, 2H, –NH₂), 6.88 (d, 1H, *J* = 16.1 Hz, –CH=C), 6.98 (dd, 1H, *J*₁ = 9.0 Hz, *J*₂ = 16.1 Hz, –CH=C), 6.99 (d, 1H, *J* = 4.0 Hz, –CH–furan), 7.69 (s, 1H, *J* = 9.4 Hz, –CH=N), 7.71 (s, 1H, *J* = 4.0 Hz, –CH–furan), 10.47 (bs, 1H, –NH). ¹³C-NMR (dmsO-d₆, 100 MHz) (HMQC and HMBC experiments): δ 113.78, 116.35, 121.53, 131.67, 140.53, 152.05, 156.04, 157.06. NOE-experiment (dmsO-d₆, *t*_{mixt} = 750 ms, irrad = 10.47 ppm, acopl (% NOE-effect): 6.98 (1.00), 7.69 (39.24).

2.2. Syntheses of the complexes [Ru^{II}Cl₂(dmsO)₂L]

[Ru^{II}Cl₂(dmsO)₄] (100 mg, 0.21 mmol) and **L** (0.42 mmol) were heated under reflux in EtOH (for **L1** and **L3**) or in C₆H₅CH₃ (for **L2**) during 8–10 h, after which a solid precipitated. The solid was filtered off and recrystallized.

2.2.1. [Ru^{II}Cl₂(dmsO)₂L1]

Yield: 77 mg, 71% (crude product). *Anal.* Calc. for C₁₀H₁₈Cl₂N₄O₆RuS₂: C, 22.9; H, 3.4; N, 10.7; S, 12.2. Found: C, 22.7; H, 3.4; N, 10.5; S, 12.4%. λ_{max} (acetone): 337, 468 nm. Single deep red crystals, suitable for X-ray analysis were obtained by slow evaporation at r.t. of a methanolic solution.

2.2.2. [Ru^{II}Cl₂(dmsO)₂L2]

Yield: 63 mg, 52% (crude product). *Anal.* Calc. for C₁₄H₂₆Cl₂N₄O₆RuS₂: C, 28.9; H, 4.5; N, 9.6; S, 11.0. Found: C, 28.6; H, 4.4; N, 9.8; S, 11.1%. λ_{max} (acetone): 334, 467 nm. Single orange crystals, suitable for X-ray analysis were obtained by slow evaporation at r.t. of a methanolic solution.

2.2.3. [RuCl₂(dmsO)₂L3]

Yield: 80 mg, 70% (crude product). *Anal.* Calc. for C₁₂H₂₀Cl₂N₄O₆RuS₂: C, 26.1; H, 3.6; N, 10.1; S, 11.6. Found: C, 26.3; H, 3.7; N, 10.1; S, 11.8%. λ_{max} (acetone): 370, 481 nm. Dark red crystals were obtained from hot EtOH.

2.3. Characterization

C, H, N and S analyses were performed with a Carlo Erba Model EA1108 elemental analyzer. FTIR spectra (4000–400 and 500–200 cm⁻¹) of the complexes and the free ligands were measured either as KBr or CsI pellets with a Bomen FTIR model M102 instrument. Electronic spectra were recorded on a Spectronic 3000 spectrophotometer. ¹H and ¹³C NMR spectra of the free ligands and of the complexes were recorded on a Bruker DPX-400 instrument (at 400 and 100 MHz, respectively). Experiments were performed at 30 °C in dmsO-d₆ (stability of

the complex in such medium was previously stated). Heteronuclear correlation experiments (2D-HETCOR), HMQC (multiple quantum) and HMBC (multiple bond), were performed with the same instrument. NOE-diff experiments were performed using the equipment's NOE-diff pulse sequences at 30 °C. The mixing time (t_{mix}) was varied from 250 to 750 ms.

Theoretical calculations were performed using the PC SPARTAN *Pro* package [16]. Complexes were built according to standard bond lengths and angles using molecular modeling package. The structure of each compound was fully optimized by molecular mechanics methods (SYBYL molecular mechanics force fields) and then by PM3 semi-empirical method. Crystallographic data for complexes $[\text{Ru}^{\text{II}}\text{Cl}_2(\text{dmsO})_2\text{L1}]$ and $[\text{Ru}^{\text{II}}\text{Cl}_2(\text{dmsO})_2\text{L2}]$ were used as template to validate the PM3 calculation. From each minimized structure a single point calculation was applied (in vacuo) using the standard PM3 algorithm.

2.4. X-ray diffraction data and crystal structure determination and refinement

Crystal data, data collection procedure, structure determination methods and refinement results for both complexes are summarized in Table 1.

The butyl substituent of $[\text{RuCl}_2(\text{dmsO})_2\text{L2}]$ appeared disordered in the electron density map. This residual density was modeled in terms of two conformations and refined such as their occupancies added up to one. During the refinement, the C–C bond and alternated C···C distances along the butyl $\text{CH}_2\text{--CH}_2\text{--CH}_2\text{--CH}_3$ chain were restrained to target values of 1.50(2) and 2.44(2) Å, respectively. Most hydrogen atoms in both **RuL1** and **RuL2** compounds were found in a difference Fourier map. However, all H-atoms but the ones of the disordered butyl group in $[\text{RuCl}_2(\text{dmsO})_2\text{L2}]$ were included in the molecular model at stereo chemical positions and refined with the riding model. The methyl hydrogen atoms of the dimethylsulfoxide ligands were treated in the refinement as rigid bodies and they were allowed to rotate along the corresponding C–S bond so as to maximize the sum of the observed electron density at the three calculated H-positions.

3. Results and discussion

Three new Ru(II) 5-nitrofurylsemicarbazone complexes were synthesized and characterized. Complexes of general formula $[\text{Ru}^{\text{II}}\text{Cl}_2(\text{dmsO})_2\text{L}]$, where **L** = 5-nitro-2-furaldehyde semicarbazone (**RuL1**), *N*⁴-n-butyl-5-nitro-2-furaldehyde semicarbazone (**RuL2**) and 3-(5-nitrofuryl)acroleine semicarbazone (**RuL3**), were prepared in good yields and high purity.

Significant vibration bands of the ligands and their metal complexes, useful for determining the ligands' mode of coordination, could be tentatively assigned and they are given in Table 2.

After coordination, the $\nu(\text{CO})$ and the $\nu(\text{C=N})$ bands of the semicarbazone free ligands, at approximately 1660–1700 and approximately 1580 cm^{-1} , respectively, shift to lower frequencies. These modifications are consistent with bidentate coordination of the semicarbazone ligands through the carbonylic oxygen and the azomethinic nitrogen. The $\nu(\text{NH})$ band at approximately 3120–3150 cm^{-1} is present in all complexes, indicating that, in the solid state, the ligand remains protonated [14,21]. In addition, the $\nu(\text{SO})$ band, observed at approximately 1100 cm^{-1} in the three complexes, confirms the presence of sulfur-bonded dmsO in the Ru coordination sphere [22]. Each complex shows four new bands in the low frequency region at approximately 320, 350, 400 and 450 cm^{-1} , that could be tentatively assigned to Ru–ligand vibrations [14,23].

3.1. Structural results

The X-ray diffraction study shows that the complexes $[\text{RuCl}_2(\text{dmsO})_2\text{L1}]$ and $[\text{RuCl}_2(\text{dmsO})_2\text{L2}]$ consist of discrete monomeric molecules. There are two different complexes per asymmetric unit, with quite similar conformations, in the $[\text{RuCl}_2(\text{dmsO})_2\text{L1}]$ crystal. Relevant intra-molecular bond distances and angles around the metal ion are shown in Tables 3 and 4, respectively. Figs. 3 and 4 are ORTEP [24] drawings of the molecules.

In **RuL1** and **RuL2** complexes, the Ru(II) ions are in an elongated octahedral environment, equatorially coordinated to **L** molecule, acting as a bidentate ligand through its azomethinic nitrogen and carbonylic oxygen atoms, and to the sulfur atoms of two dimethylsulfoxide (dmsO) groups at *cis* positions. The octahedral coordination is completed with a pair of chlorine ions at the axial positions. In **RuL1** complexes, the equatorial NOS_2 group of ligands are planar to within experimental accuracy, with the ruthenium ion laying on the plane. The nitrofurane heterocycle and terminal NO_2 planes are coplanar with the corresponding equatorial NOS_2 plane. For **RuL2**, the nitrofurane heterocycle plane is tilted in 1.8(5)° from the equatorial NOS_2 plane. The NO_2 plane, in turn, is tilted from the heterocycle plane in 4.7(5)°.

Complexes were obtained by substitution onto the precursor $[\text{RuCl}_2(\text{dmsO})_4]$. In the latter, both Cl ligands take mutually *cis* positions [22]. Interestingly, substitution of two dmsO ligands by **L1** or **L2** leads to *trans*-dichloro ruthenium complexes. Ru–S bond lengths are quite similar to those reported for other Ru(II)–S–dmsO mixed ligand complexes [22,25]. Owing to coordination, some changes in dmsO moiety are observed. For **RuL1**, S–O bond lengths vary from 1.472 to 1.523 Å. For

Table 1

Crystal data and structure solution methods and refinement results for [RuCl₂(dms_o)₂L1], (**RuL1**), and [RuCl₂(dms_o)₂L2], (**RuL2**), complexes

	RuL1	RuL2
Empirical formula	C ₁₀ H ₁₈ Cl ₂ N ₄ O ₆ RuS ₂	C ₁₄ H ₂₆ Cl ₂ N ₄ O ₆ RuS ₂
Formula weight	525.36	581.47
Temperature (K)	120(2)	120(2)
Low-temperature device	Oxford Cryosystems	Oxford Cryosystems
Cooling rate	200 K h ⁻¹	200 K h ⁻¹
Crystal system	monoclinic	triclinic
Space group	<i>P</i> 2 ₁ / <i>c</i>	<i>P</i> - $\bar{1}$
Unit cell dimensions ^a		
<i>a</i> (Å)	8.189(1)	8.4320(1)
<i>b</i> (Å)	31.806(6)	12.5870(2)
<i>c</i> (Å)	13.964(4)	12.7580(2)
α (°)	90.00	63.936(1)
β (°)	90.759(9)	74.044(1)
γ (°)	90.00	87.947(1)
<i>V</i> (Å ³)	3637(1)	1163.82(3)
<i>Z</i>	8	2
Calculated density (Mg m ⁻³)	1.919	1.659
Absorption coefficient, μ (mm ⁻¹)	1.421	1.119
<i>F</i> (000)	2104	590
Crystal size (mm)	0.06 × 0.04 × 0.04	0.32 × 0.13 × 0.12
Crystal color/shape	red/hexagonal	orange/prismatic
Diffractionmeter/scan	KappaCCD/ φ and ω	KappaCCD/ φ and ω
Radiation, graphite monochromator	Mo K α , λ = 0.71073 Å	Mo K α , λ = 0.71073 Å
θ Range for data collection (°)	1.28–20.00	1.81–25.00
Index ranges	−7 ≤ <i>h</i> ≤ 7, 0 ≤ <i>k</i> ≤ 30, 0 ≤ <i>l</i> ≤ 13	−9 ≤ <i>h</i> ≤ 10, −14 ≤ <i>k</i> ≤ 14, −15 ≤ <i>l</i> ≤ 15
Reflections collected	11 175	7722
Reflections observed [<i>I</i> > 2 σ (<i>I</i>)]	2351	3820
Independent reflections	3396 [<i>R</i> _{int} = 0.149]	4091 [<i>R</i> _{int} = 0.011]
Completeness	97.6% (to θ = 20°)	99.9% (to θ = 25°)
Max/min transmission	0.945 and 0.920	0.877 and 0.716
Data reduction and correction ^b and structure solution ^c and refinement programs ^d	DENZO and SCALEPACK [18], SHELXS-97 [19], SHELXL-97 [20]	DENZO and SCALEPACK [18], SHELXS-97 [19], SHELXL-97 [20]
Refinement method	full-matrix least-squares on <i>F</i> ²	full-matrix least-squares on <i>F</i> ²
Weights (<i>w</i>)	$[\sigma^2(F_o^2) + (0.041P)^2 + 47.1P]^{-1}$ $P = [\text{Max}(F_o^2, 0) + 2F_c^2]/3$	$[\sigma^2(F_o^2) + (0.081P)^2 + 0.66P]^{-1}$ $P = [\text{Max}(F_o^2, 0) + 2F_c^2]/3$
Data/restraints/parameters	3396/0/429	4091/9/281
Final <i>R</i> indices [<i>I</i> > 2 σ (<i>I</i>)] ^e	<i>R</i> ₁ = 0.066, <i>wR</i> ₂ = 0.146	<i>R</i> ₁ = 0.029, <i>wR</i> ₂ = 0.094
<i>R</i> indices (all data)	<i>R</i> ₁ = 0.116, <i>wR</i> ₂ = 0.167	<i>R</i> ₁ = 0.038, <i>wR</i> ₂ = 0.130
Goodness-of-fit on <i>F</i> ²	1.204	1.314
Largest peak and hole (e Å ⁻³)	0.89 and −1.50	1.67 and −1.74

^a Least-squares refinement of the angular settings for 148482 (**RuL1**) and 5324 (**RuL2**) reflections in the 1.02 < θ < 25.03 (**RuL1**) and 1.0 < θ < 27.5° (**RuL2**) ranges.

^b Corrections: Lorentz, polarization and absorption correction [17].

^c Neutral scattering factors and anomalous dispersion corrections.

^d Structure solved by Patterson and Fourier methods. The final molecular model obtained by anisotropic full-matrix least-squares refinement of the non-hydrogen atoms.

^e *R* indices defined as: $R_1 = \Sigma ||F_o| - |F_c|| / \Sigma |F_o|$, $wR_2 = [\Sigma w(F_o^2 - F_c^2)^2 / \Sigma w(F_o^2)]^{1/2}$.

Table 2

Selected vibration bands of the ligands and their Ru complexes (cm⁻¹)

Compound	ν (CO)	ν (C=N)	ν_s (NO ₂)	ν (SO) _{dms_o}
L1	1716	1583	1350	–
L2	1696	1576	1355	–
L3	1675	1585	1351	–
RuL1	1665	1533	1347	1078
RuL2	1651	1529	1351	1105
RuL3	1662	1533	1347	1072

ν , stretching; s, symmetric.

RuL2, a shortening in S–O bond lengths (1.483 and 1.484 Å) is observed (average value in free sulfoxides 1.492 Å), as expected for *S*-dimethylsulfoxide complexes. Observed O–S–C and C–S–C bond angles and C–S bond distances are quite similar to the previously reported values [25].

Observed Ru–O, Ru–N and Ru–Cl bond distances are quite similar to those reported for other ruthenium(II) semicarbazone complexes [14]. Ru–ligand bond lengths are slightly shorter in **RuL1** than in **RuL2**,

Table 3
Interatomic bond distances (Å) around the ruthenium for [RuCl₂(dms₂)₂L1], (**RuL1**), and [RuCl₂(dms₂)₂L2], (**RuL2**)

RuL1		RuL2	
Complex #1		Complex #2	
Ru(1)–O(11)	2.07(1)	Ru(2)–O(21)	2.08(1)
Ru(1)–N(13)	2.10(1)	Ru(2)–N(23)	2.10(1)
Ru(1)–S(11)	2.222(5)	Ru(2)–S(21)	2.189(5)
Ru(1)–S(12)	2.231(4)	Ru(2)–S(22)	2.236(4)
Ru(1)–Cl(12)	2.386(4)	Ru(2)–Cl(21)	2.382(4)
Ru(1)–Cl(11)	2.394(4)	Ru(2)–Cl(22)	2.400(4)
		Ru–O(1)	2.118(2)
		Ru–N(3)	2.113(3)
		Ru–S(1)	2.2320(9)
		Ru–S(2)	2.2452(8)
		Ru–Cl(1)	2.3938(8)
		Ru–Cl(2)	2.4100(8)

Table 4
Selected angles (°) for [RuCl₂(dms₂)₂L1], **RuL1**, and [RuCl₂(dms₂)₂L2], **RuL2**

RuL1		RuL2	
Complex #1		Complex #2	
O(11)–Ru(1)–N(13)	76.7(5)	O(21)–Ru(2)–N(23)	76.2(5)
O(11)–Ru(1)–S(11)	176.5(3)	O(21)–Ru(2)–S(21)	176.8(3)
N(13)–Ru(1)–S(11)	99.8(4)	N(23)–Ru(2)–S(21)	100.6(4)
O(11)–Ru(1)–S(12)	91.2(3)	O(21)–Ru(2)–S(22)	92.0(3)
N(13)–Ru(1)–S(12)	167.9(4)	N(23)–Ru(2)–S(22)	168.2(4)
S(11)–Ru(1)–S(12)	92.3(2)	S(21)–Ru(2)–S(22)	91.1(2)
O(11)–Ru(1)–Cl(12)	85.9(3)	O(21)–Ru(2)–Cl(21)	86.7(3)
N(13)–Ru(1)–Cl(12)	88.9(4)	N(23)–Ru(2)–Cl(21)	91.1(3)
S(11)–Ru(1)–Cl(12)	93.9(2)	S(21)–Ru(2)–Cl(21)	93.6(2)
S(12)–Ru(1)–Cl(12)	91.1(2)	S(22)–Ru(2)–Cl(21)	89.4(2)
O(11)–Ru(1)–Cl(11)	89.8(3)	O(21)–Ru(2)–Cl(22)	88.2(3)
N(13)–Ru(1)–Cl(11)	84.4(4)	N(23)–Ru(2)–Cl(22)	82.7(3)
S(11)–Ru(1)–Cl(11)	90.1(2)	S(21)–Ru(2)–Cl(22)	91.1(2)
S(12)–Ru(1)–Cl(11)	94.8(2)	S(22)–Ru(2)–Cl(22)	96.0(2)
Cl(12)–Ru(1)–Cl(11)	172.8(2)	Cl(21)–Ru(2)–Cl(22)	172.8(2)
		N(3)–Ru–O(1)	77.5(1)
		O(1)–Ru–S(1)	176.13(6)
		N(3)–Ru–S(1)	98.83(8)
		O(1)–Ru–S(2)	89.02(7)
		N(3)–Ru–S(2)	166.37(8)
		S(1)–Ru–S(2)	94.68(3)
		O(1)–Ru–Cl(1)	89.65(7)
		N(3)–Ru–Cl(1)	84.94(8)
		S(1)–Ru–Cl(1)	91.28(3)
		S(2)–Ru–Cl(1)	93.01(3)
		O(1)–Ru–Cl(2)	87.70(7)
		N(3)–Ru–Cl(2)	90.38(8)
		S(1)–Ru–Cl(2)	91.10(3)
		S(2)–Ru–Cl(2)	91.15(3)
		Cl(1)–Ru–Cl(2)	175.02(3)

indicating slightly stronger bonds in the former complex.

It is interesting to note that during the formation of the five-membered chelate rings, the semicarbazone ligands suffer a stereochemical change around the C=N bond, relative to the free ligand structures. So, although the free ligands exist as the isomeric form *E*, X-ray diffraction studies show that upon coordination the ligands adopt the isomeric form *Z* [12,26]. Bond distances within the semicarbazone ligand, particularly the corresponding to the C–O bond [RuL1: 1.245(19) complex #1, 1.212(18) complex #2 and RuL2 1.249(4) Å], together with the presence of the N–H proton clearly indicate that the semicarbazone ligand is bound to ruthenium in the keto form [14].

In **RuL1**, complexes #1 and #2 are stabilized by intramolecular N(amide)–H···O bonds. The crystal is further stabilized by a net of intermolecular N(amide)–H···O bonds involving the dimethylsulfoxide oxygen atoms. In **RuL2**, the heterocycle of the semicarbazone ligand is rotated in about 180° compared to that in **RuL1** (see Fig. 2). Therefore, no intramolecular N(amide)–H···O bond is present in the former com-

plex. The **RuL2** crystal is stabilized by a net of intermolecular N–H···Cl bonds. H-bond distances and angles are detailed in the supplementary Tables S12 and S13.

3.2. NMR studies

The NMR experiments show narrow signals, typical for Ru(II) diamagnetic complexes. HETCOR experiments allowed to assign all signals of the free ligands and the investigated complexes. ¹H NMR integrations and signal multiplicities are in agreement with the proposed formula (Table 5). The attached figure shows the numbering scheme of the free ligands mentioned in the Tables and the text. The three complexes show similar ¹H and ¹³C chemical shifts of the nitrofurylsemicarbazone common portion of their molecules. When the ligand is coordinated, a downfield shifting of all the ¹H NMR peaks, including those of the dms₂ ligand (free dms₂ δ-H = 2.50 ppm) is observed. The chemical shift differences between each complex and the corresponding ligand, expressed as Δδ, are shown in Table 5. Such differences may be partially caused by the change in the

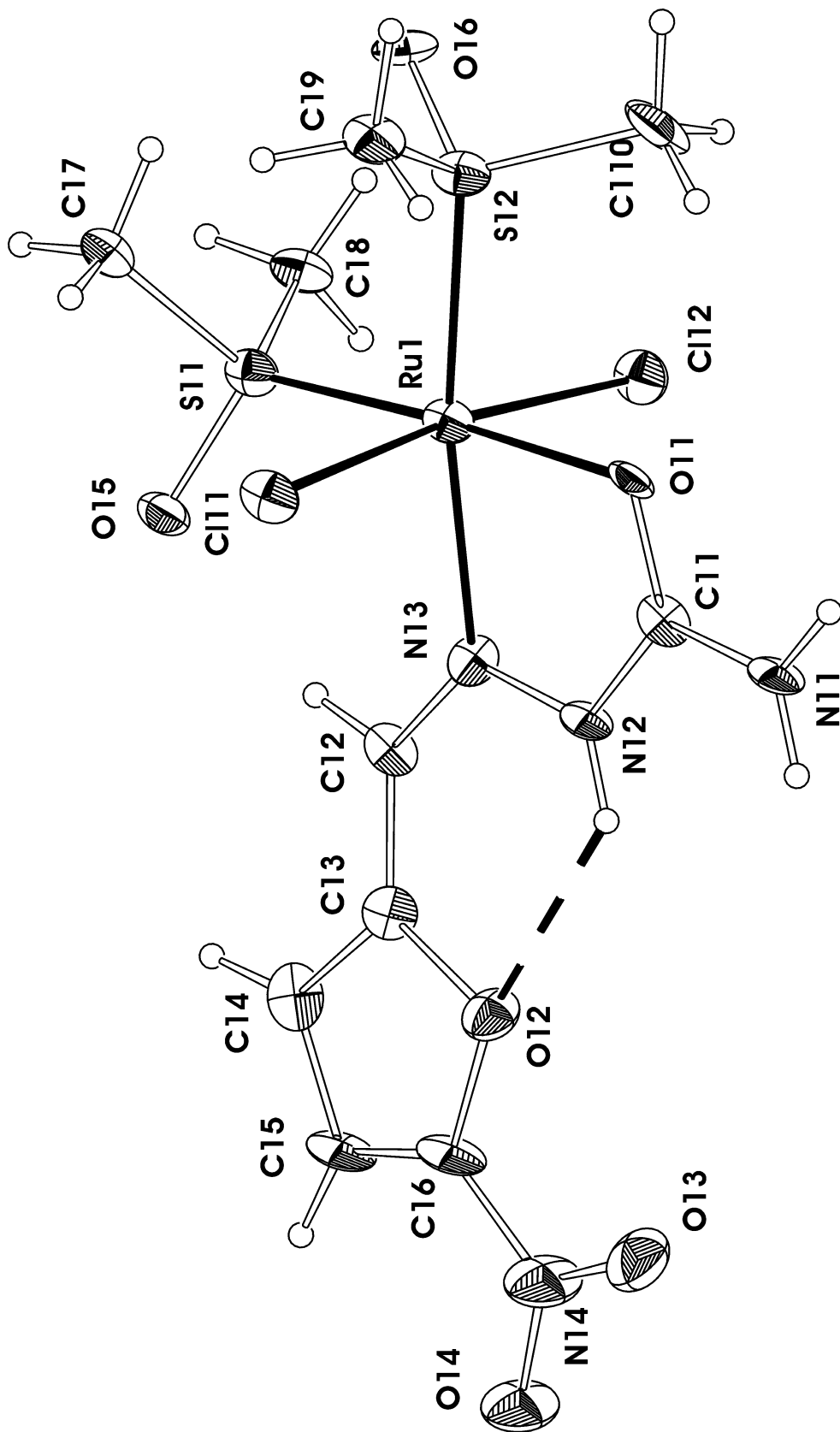


Fig. 3. View of one of the two independent complexes in the asymmetric unit of $[\text{Ru}^{\text{II}}\text{Cl}_2(\text{dms})_2\text{L1}]$ showing the labeling scheme of the non-H atoms and their displacement ellipsoids at the 30% probability level. Ru–ligand bonds are indicated by full lines and the intra-molecular H-bond with a dashed line.

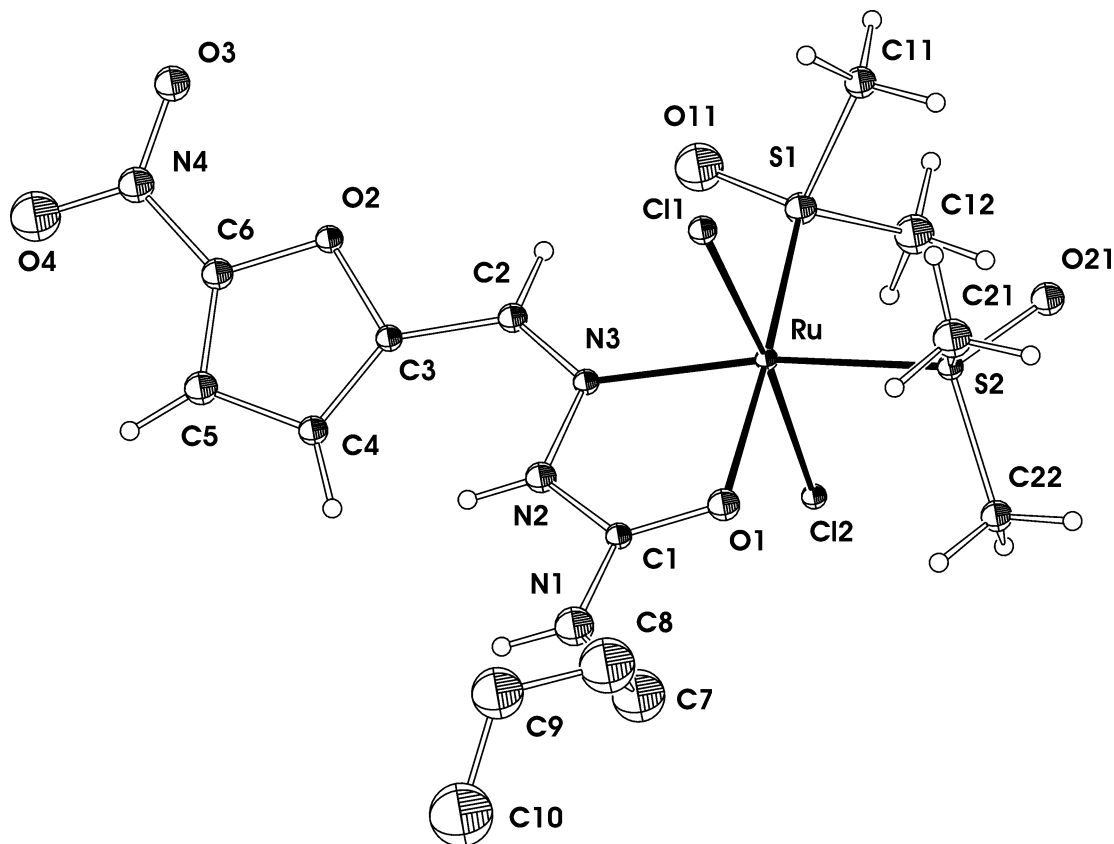


Fig. 4. Molecular plot of $[\text{Ru}^{\text{II}}\text{Cl}_2(\text{dms})_2\text{L}_2]$. The drawing shows only one of the conformations of the disordered butyl $\text{CH}_2\text{CH}_2\text{CH}_2\text{CH}_3$ group.

ligands conformation (from *E* to *Z* form). However, when comparing *E* form of related 5-nitrofurano analogues compounds to their *Z* form, very small chemical shifts of the furanic and azomethynic protons are observed (less than 0.2 ppm) [27]. Furthermore, in all complexes, largest $\Delta\delta$ are observed for the protons that are located close to the coordinating atoms (azomethynic nitrogen and carbonylic oxygen), i.e. protons 7, 8, and 10. So, the deshielding effect of the metal is apparent to such protons.

Upon coordination, the most distinguishing feature of the ^{13}C NMR spectra is the change in the chemical shifts of the carbons numbered 1, 3, 5, 7 (**RuL1** and **RuL2**) and 1, 3, 5, 7 and 9 (**RuL3**). While the signals of all protons are significantly displaced downfield owing to an electron attractive effect of the metal, these effects are only observed in the mentioned carbons. These could be explained through an electron delocalization process that would favor an increase in the electronic density of the coordinating atoms. This process would produce an electronic density decrease in the mentioned carbon atoms and hence a deshielding.

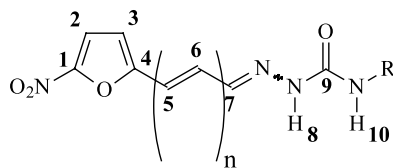
A comparison of **RuL1** and **RuL2** ^1H NMR and NOE spectra with that of **RuL3** makes it possible to obtain some structural features about the latter. Experiments

seem to indicate that, in solution, the three complexes show the same spatial distribution of the ligands. Concerning the geometry, a *trans,cis,cis*- $\text{RuCl}_2(\text{dms})_2\text{L}$ complex is also expected for **L3** since only two different ^1H NMR dms signals are observed for the three complexes. In addition, NOE spectra show $\text{H}_7\text{--H}_3$ spatial coupling and both protons also couple spatially to dms ligand protons. Even for **RuL3**, where H_3 is farther from H_7 and H_{dms} , this spatial coupling is observed (Table 6).

RuL1 and **RuL2** show different preferential conformations of the nitrofurano group in the solid state. However, no conclusions about complexes conformation in solution can be obtained from NOE experiments. Even though, for these complexes, H_3 does not couple spatially to H_8 , such coupling could not be detected because of the widening of H_8 signal. Despite these facts, due to free rotation, no preferential nitrofurano spatial distribution should be expected in solution.

For **RuL1** and **RuL2**, the detection of $\text{H}_7\text{--H}_{\text{dms}}$ spatial coupling confirms the *Z* form around **L**-azomethynic moiety observed in their crystal structures (even though the free ligands present the *E* conformation, as confirmed by NOE experiments [12,26]). For **RuL3** the *Z* form around the azomethynic moiety can

Table 5

 ^1H and ^{13}C NMR chemical shift values (δ) in ppm of **L** and $[\text{Ru}^{\text{II}}\text{Cl}_2(\text{dmsO})_2\text{L}]$, with **L** = **L1**, **L2** and **L3**, in $\text{dmsO}-d_6$ at 303 K

^1H NMR	L1 ($n = 0$, $\text{R} = \text{H}$) ^a		L2 ($n = 0$, $\text{R} = \text{butyl}$) ^{a,b}		L3 ($n = 1$, $\text{R} = \text{H}$) ^a		$\Delta\delta$ ^c		
	δ_{Ligand}	δ_{Complex}	δ_{Ligand}	δ_{Complex}	δ_{Ligand}	δ_{Complex}	$\Delta\delta_{\text{L1}}$	$\Delta\delta_{\text{L2}}$	$\Delta\delta_{\text{L3}}$
2	7.75	7.95	7.76	7.95	7.71	7.79	0.20	0.19	0.08
3	7.21	7.70	7.20	7.70	6.99	7.18	0.49	0.50	0.19
5	–	–	–	–	6.88	7.20	–	–	0.32
6	–	–	–	–	6.98	7.46	–	–	0.48
7	7.80	9.34	7.79	9.31	7.69	8.98	1.54	1.52	1.29
8	10.76	11.40	10.81	11.36	10.47	11.79	0.64	0.55	1.32
10	6.57	7.85	6.92	8.29	6.40	7.37	1.28	1.37	0.97
11	–	–	3.13	3.33	–	–	–	0.20	–
12	–	–	1.45	1.51	–	–	–	0.06	–
13	–	–	1.28	1.35	–	–	–	0.07	–
14	–	–	0.89	0.89	–	–	–	0.00	–
dmsO ^d	–	3.28	–	3.29	–	3.25	0.78	0.79	0.75
	–	3.29	–	–	–	3.27	0.79	–	0.77
^{13}C NMR	L1 ($n = 0$, $\text{R} = \text{H}$)		L2 ($n = 0$, $\text{R} = \text{butyl}$) ^e		L3 ($n = 1$, $\text{R} = \text{H}$)		$\Delta\delta$ ^f		
	δ_{Ligand}	δ_{Complex}	δ_{Ligand}	δ_{Complex}	δ_{Ligand}	δ_{Complex}	$\Delta\delta_{\text{L1}}$	$\Delta\delta_{\text{L2}}$	$\Delta\delta_{\text{L3}}$
1	152.00	152.36	152.13	152.32	152.05	153.50	0.36	0.19	1.45
2	115.95	114.87	116.06	114.87	116.35	116.00	–1.08	–1.19	–0.35
3	112.80	120.28	113.26	120.32	113.78	118.70	7.48	7.06	4.92
4	154.00	146.40	153.89	146.47	156.04	154.20	–7.60	–7.42	–1.84
5	–	–	–	–	121.53	128.00	–	–	6.47
6	–	–	–	–	131.67	120.00	–	–	–11.67
7	128.45	138.84	128.24	138.97	140.53	150.50	10.39	10.73	9.97
9	157.00	163.91	155.54	162.92	157.06	162.50	6.91	7.38	5.44
11	–	–	39.66	41.32	–	–	–	1.66	–
12	–	–	32.83	32.01	–	–	–	–0.82	–
13	–	–	20.36	20.21	–	–	–	–0.15	–
14	–	–	14.55	14.44	–	–	–	–0.11	–
dmsO ^g	–	45.73	–	45.75	–	46.55	5.13	5.15	5.95
	–	45.85	–	45.91	–	46.85	5.25	5.31	6.25

^a Integration: **RuL1**: $\text{H}_2:\text{H}_3:\text{H}_7:\text{H}_8:\text{H}_{10}:\text{H}_{\text{dmsO}} = 1:1:1:1:2:12$; **RuL2**: $\text{H}_2:\text{H}_3:\text{H}_7:\text{H}_8:\text{H}_{10}:\text{H}_{11}:\text{H}_{12}:\text{H}_{13}:\text{H}_{14}:\text{H}_{\text{dmsO}} = 1:1:1:1:1:2:2:3:12$; **RuL3**: $\text{H}_2:\text{H}_3:\text{H}_5:\text{H}_6:\text{H}_7:\text{H}_8:\text{H}_{10}:\text{H}_{\text{dmsO}} = 1:1:1:1:1:1:2:12$.

^b With $\text{R} = -\text{CH}_2(\mathbf{11})-\text{CH}_2(\mathbf{12})-\text{CH}_2(\mathbf{13})-\text{CH}_3(\mathbf{14})$.

^c $\Delta\delta = (\delta_{\text{Complex}} - \delta_{\text{Ligand}})$.

^d $\delta_{\text{H-dmsO}} = 2.50$ ppm.

^e With $\text{R} = -\text{C}(\mathbf{11})\text{H}_2-\text{C}(\mathbf{12})\text{H}_2-\text{C}(\mathbf{13})\text{H}_2-\text{C}(\mathbf{14})\text{H}_3$.

^f $\Delta\delta = (\delta_{\text{Complex}} - \delta_{\text{Ligand}})$.

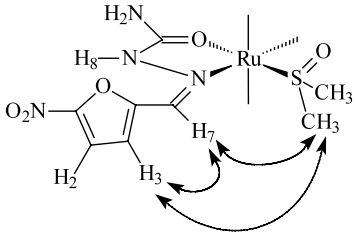
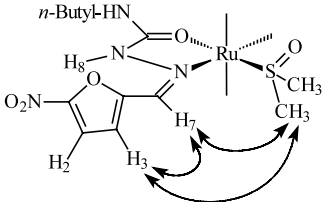
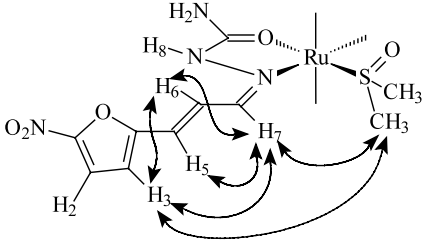
^g $\delta_{\text{C-dmsO}} = 40.60$ ppm.

also be predicted even though crystal structure is not available. $\text{H}_7-\text{H}_{\text{dmsO}}$ spatial coupling is observed, as in the other complexes. In addition, when H_8 is irradiated, no H_7 -spatial coupling is detected in the selected experimental conditions. Using the same mixing time in the NOE experiments for the free ligand (**L3**), H_8 shows spatial coupling to H_7 , thus confirming the

conformation change of the ligand due to the complex formation.

Semi empirical studies were performed in an effort to confirm, in thermodynamic terms, this change in ligand spatial distribution. For the three complexes theoretical calculations in vacuo, using PM3 algorithm, on the *E* and *Z* isomers were performed. In all cases, calculations

Table 6
NOE-diff experiments, relevant spatial couplings

Complex ^(a)	Irradiated H	t_{mixture} (ms)	Spatial coupling	% of NOE effect
			H ₇	0.41
	H ₃	500	H _{dmso}	2.82
	H ₇	500	H ₃	0.22
			H _{dmso}	0.42
	H ₃	500	H _{dmso}	1.60
			H ₃	0.29
	H ₇	500	H _{dmso}	0.31
			H ₆	0.73
	H ₃	750	H ₇	0.42
			H _{dmso}	0.02
			H ₃	0.59
	H ₇	750	H ₅	0.61
			H ₆	0.19
		H _{dmso}	1.39	

(a) Chlorine and one dmsO ligands are omitted for simplicity.

indicate that the *E*-form of the ligand results in a higher energy level of each complex than the *Z* stereoisomeric form (Table 7).

Although crystal structure of **RuL3**, where **L3** = 3-(5-nitro-2-furyl)acroleine semicarbazone, has not been solved yet, proposed formula for this complex is [Ru^{II}Cl₂(dmsO)₂L3]. Support for the proposed stoichiometry was obtained from satisfactory elemental analysis results and ¹H NMR integrations. Support for the

ligand spatial configuration and proposed coordinating atoms was obtained from detailed FTIR and NMR spectroscopic studies and theoretical calculations. **L3**, as the *Z* form around the azomethynic moiety, is likely to bind to the metal through the carbonylic oxygen and the azomethynic nitrogen atoms, as in the other complexes.

The effect of these new complexes on the proliferation of *in vitro* cultures of *T. cruzi* is being evaluated and these results will be the subject of future publications.

Table 7
Energy calculations

Complex	Energy/kcal mol ⁻¹		$\Delta E/\text{kcal mol}^{-1}$ ^a
	<i>E</i> -L	<i>Z</i> -L	
RuL1	-286.46	-306.94	-20.48
RuL2	-327.27	-345.08	-17.81
RuL3	-281.43	-293.86	-12.43

^a $\Delta E = E[\text{RuCl}_2(\text{dmsO})_2\text{-Z-L}] - E[\text{RuCl}_2(\text{dmsO})_2\text{-E-L}]$.

4. Supplementary material

Fractional coordinates and equivalent isotropic displacement parameters (Tables S1 and S2), listings of full bond distances and angles (Tables S3 and S4), atomic anisotropic thermal parameters (Tables S5 and S6), hydrogen atoms positions (Tables S7 and S8), H-bonds distances and angles (Tables S9 and S10) and calculated and observed structure factor amplitudes (Table S11

and S12). Crystallographic data for the structural analysis have been deposited with the Cambridge Crystallographic Data Centre, CCDC No. 181913 and 181914 for compounds $[\text{RuCl}_2(\text{dmsO})_2\text{L1}]$ and $[\text{RuCl}_2(\text{dmsO})_2\text{L2}]$, respectively. Copies of this information may be obtained free of charge from The Director, CCDC, 12 Union Road, Cambridge, CB2 1EZ, UK (fax: +44-1223-336033; e-mail: deposit@ccdc.cam.ac.uk or www: <http://www.ccdc.cam.ac.uk>).

Acknowledgements

This work was supported by PEDECIBA and CONICYT of Uruguay, TWAS, FAPESP of Brazil and by the collaborative agreement between CONICET of Argentina and CNPq of Brazil.

References

- [1] M.S. Braga, L. Lauria-Pires, E.R. Argañaraz, R.J. Nascimento, A.R. Teixeira, *Rev. Inst. Med. Trop. Sao Paulo* 42 (2000) 157.
- [2] N.B. Gorla, O.S. Ledesma, G.P. Barbieri, I.B. Larripa, *Mutat. Res.* 2241 (1989) 263.
- [3] C. Olea-Azar, A.M. Atria, F. Mendizabal, R. Di Maio, I. Caracalli, G. Seoane, H. Cerecetto, *Spectrosc. Lett.* 31 (1998) 99.
- [4] H. Cerecetto, R. Di Maio, G. Ibarruri, G. Seoane, A. Denicola, C. Quijano, G. Peluffo, M. Paulino, *Farmaco* 53 (1998) 89.
- [5] N. Farrell, *Transition Metal Complexes as Drugs and Chemotherapeutic Agents*, vol. 11, Kluwer Academic Publishers, London, 1989, p. 230.
- [6] G. Maestroni, E. Alessio, G. Sava, S. Pacor, M. Coluccia, *Metal Complexes in Cancer Chemotherapy*, VCH, Weinheim, 1993, pp. 159–185.
- [7] R. Sánchez Delgado, K. Lazard, L. Rincón, J. Urbina, *J. Med. Chem.* 36 (1993) 2041.
- [8] R. Sánchez Delgado, M. Navarro, K. Lazard, R. Atencio, M. Caparelli, F. Vargas, J. Urbina, A. Boulliez, A. Noels, D. Masi, *Inorg. Chim. Acta* (1998) 275.
- [9] M. Navarro, T. Lehman, E. Cisneros-Fajardo, A. Fuentes, R. Sánchez Delgado, J. Urbina, *Polyhedron* 19 (2000) 2319.
- [10] A.J. Castilla, C.M. Mesa-Valle, M. Sanchez Moreno, T. Arnedo, M. Rosales, C. Mascaro, D. Craciunescu, A. Osuna, *Arzneim.-Forsch/Drug Res.* 46 (1996) 990.
- [11] C.M. Mesa-Valle, V. Moradela, D. Craciunescu, M.P. Alonso, A. Osuna, *Arzneim.-Forsch/Drug Res.* 43 (1993) 1010.
- [12] H. Cerecetto, R. Di Maio, M. González, M. Risso, G. Sagraera, G. Seoane, A. Denicola, G. Peluffo, C. Quijano, A. Stoppani, M. Paulino, C. Olea-Azar, M.A. Basombrio, *Eur. J. Med. Chem.* 35 (2000) 343.
- [13] G. Henderson, P. Ulrich, A. Fairlamb, I. Rosemberg, M. Pereira, M. Sela, A. Cerami, *Proc. Natl. Acad. Sci. USA* 85 (1998) 5374.
- [14] F. Basuli, S. Peng, S. Battacharya, *Inorg. Chem.* 40 (2001) 1126.
- [15] I. Evans, A. Spencer, G. Wilkinson, *J. Chem. Soc., Dalton Trans.* (1973) 204.
- [16] Wavefunction, Inc., 18401 Von Karman Avenue, Suite 370, Irvine, CA 92612, USA.
- [17] R.H. Blessing, *Acta Crystallogr.*, A 51 (1995) 33.
- [18] Z. Otwinowski, W. Minor, *Methods in Enzymology*, vol. 276, Academic Press, New York, 1997, pp. 307–326.
- [19] G.M. Sheldrick, *SHELXS-97*. Program for Crystal Structure Resolution, University of Göttingen, Göttingen, Germany, 1997.
- [20] G.M. Sheldrick, *SHELXL-97*. Program for Crystal Structures Analysis, University of Göttingen, Göttingen, Germany, 1997.
- [21] El Mostapha Jouad, A. Riou, M. Allain, M. A. Khan, G. Bouet, *Polyhedron* 20 (2001) 67.
- [22] E. Alessio, G. Mestroni, G. Nardin, W. Attia, M. Calligaris, G. Sava, S. Zorzet, *Inorg. Chem.* 27 (1988) 4099.
- [23] S. Padhyé, G. Kauffman, *Coord. Chem. Rev.* 63 (1985) 127.
- [24] C.K. Johnson, *ORTEP*, Report ORNL-3794, Oak Ridge, TN, 1965.
- [25] M. Calligaris, O. Carugo, *Coord. Chem. Rev.* 153 (1996) 83.
- [26] H. Wolfgang, *Arch. Pharm.* 325 (1992) 769.
- [27] H. Cerecetto, M. Gonzalez, unpublished results.